https://ntrs.nasa.gov/search.jsp?R=19950022387 2020-06-16T07:49:55+00:00Z

# Interim Progress Report on NASA Grant NAG5-2232

## "Receiver Design, Performance Analysis, and Evaluation for Space-Borne Laser Altimeters and Space-to-Space Laser Ranging Systems"

for the period of October 16, 1994 to April 15, 1995

*Frederic M. Davidson*
*Xiaoli Sun*
*Christopher T. Field*

May 1995

Department of Electrical and Computer Engineering
The Johns Hopkins University, Baltimore, MD 21218-2686

## *SUMMARY*

This Interim report consists of three separate reports: "Laser Altimeter Ranging Error versus Received Pulse Width and Amplitude for Leading Edge, Half Width, and Centroid Detection," "Final Report on GAMES Master Oscillator," and "Sample Rate and Number of Bits Required for the GLAS Waveform Digitizer."

# Laser Altimeter Ranging Error versus Received Pulse Width and Amplitude for Leading Edge, Half Width, and Centroid Detection

*Xiaoli Sun*
Dept. ECE, Johns Hopkins University
May 1995

## 1. Introduction

Laser altimeters measure the time of flight of the laser pulses to determine the range of the target. The simplest altimeter receiver consists of a photodetector followed by a leading edge detector. A time interval unit (TIU) measures the time from the transmitted laser pulse to the leading edge of the received pulse as it crosses a preset threshold. However, the ranging error of this simple detection scheme depends on the received, pulse amplitude, pulse shape, and the threshold. In practice, the pulse shape and the amplitude are determined by the target target characteristics which has to be assumed unknown prior to the measurement. The ranging error can be improved if one also measures the pulse width and use the average of the leading and trailing edges (half pulse width) as the pulse arrival time. The ranging error becomes independent of the received pulse amplitude and the pulse width as long as the pulse shape is symmetric. The pulse width also gives the slope of the target. The ultimate detection scheme is to digitize the received waveform and calculate the centroid as the pulse arrival time. The centroid detection always gives unbiased measurement even for asymmetric pulses. In this report, we analyze the laser altimeter ranging errors for these three detection schemes using the Mars Orbital Laser Altimeter (MOLA) as an example.

## 2. Leading Edge Detection

The standard deviation of the ranging error for leading edge detection is given by

$$\sigma_r = 2\frac{\sigma_t}{c} \tag{1}$$

where $\sigma_t$ is the rms jitter in threshold crossing time and $c$ is the speed of light. To obtain $\sigma_t$, let us denote the photodetector output as $i_{pd}(t)$, and define the signal and the noise as

$$\begin{aligned} s(t) &= < i_{pd}(t) > \\ n(t) &= i_{pd}(t) - < i_{pd}(t) > \end{aligned} \tag{2}$$

Let $s_{th}$ and $T_R$ be the threshold level and the average leading edge threshold crossing time, approximate $s(t)$ by the first two terms of its Taylor expansion about $T_R$. The threshold crossing time, $t_R$, can be written as the solution to the equation

$$\begin{aligned} s_{th} &= s(t_R) + n(t_R) \\ &\approx s(T_R) + s'(T_R)(t_R - T_R) + n(t_R) \end{aligned} \tag{3}$$

Since $s_{th} \equiv s(T_R)$, $(t_R - T_R) \approx -n(t_R)/s'(T_R)$, the variance of the threshold crossing time becomes

$$\sigma_t^2(T_R) = < (t_R - T_R)^2 > = \frac{\sigma_n^2(T_R)}{[s'(T_R)]^2} \tag{4}$$

with $\sigma_n^2(t)$ the variance of the total noise at time $t$.

Let us define the signal as the number of primary photoelectrons accumulated over the equivalent integration time of the lowpass filter, $\tau_n$. The signal can be written as[1]

$$s(t) = \bar{n} G \tau_n \int_{-\infty}^{\infty} h(\tau) p(t - \tau) d\tau \tag{5}$$

with $\bar{n}$ the average number of detected photons per pulse, $G$ the average gain of the photodetector (usually an APD), $h(t)$ the impulse response of the lowpass filter before the discriminator, $\int_0^{\infty} h(t)dt = 1$,

[1] D. L. Snyder, *Random Point Processes*, John Wiley & Sons, New York, 1975, p. 171.

and $p(t)$ the normalized pulse shape function, $\int_{-\infty}^{\infty} p(t)dt = 1$. The one sided noise bandwidth of the lowpass filter is given by

$$BW_n = \frac{1}{2} \cdot \frac{1}{2\pi} \int_{-\infty}^{\infty} |H(\omega)|^2 d\omega = \frac{1}{2} \int_{0}^{\infty} h^2(t)dt \tag{6}$$

The equivalent integration time of the lowpass filter is given by

$$\tau_n = \frac{1}{2BW_n} \tag{7}$$

The derivative of the signal is given by

$$s'(t) = \bar{n} G \tau_n \int_{-\infty}^{\infty} h(\tau) p'(t-\tau) d\tau \tag{8}$$

For Gaussian pulse shape,

$$p(t) = \frac{1}{\sqrt{2\pi}\sigma_L} e^{-t^2/2\sigma_L^2}, \qquad p'(t) = \frac{1}{\sqrt{2\pi}\sigma_L} \frac{-t}{\sigma_L^2} e^{-t^2/2\sigma_L^2} \tag{9}$$

where $\sigma_L$ is the rms pulse width. Here, we assumed the received pulses arrive at $t=0$. Note the rms pulse width is related to the FWHM pulse width, $T_{FWHM}$, by

$$\sigma_L = \frac{T_{FWHM}}{2\sqrt{2\ln(2)}} = 0.85 \times \frac{T_{FWHM}}{2} \tag{10}$$

The impulse response of the lowpass filter is determined by the actual filter used. The bandwidth of the APD and the preamplifier is assumed much wider than that of the lowpass filter. Appendix A shows how the impulse response function was obtained for a 5 pole Bessel lowpass filter.

The threshold level, $s_{th}$, is set such that the receiver false alarm rate does not exceed a certain level over a given range gate interval. Appendix B shows a detailed derivation of the optimal threshold level using MOLA as an example. The average threshold crossing time at the leading edge, $T_R$, is the first of the two roots to the equation

$$s(T_R) - s_{th} = \bar{n} G \tau_n \int_{-\infty}^{\infty} h(\tau) p(T_R - \tau) d\tau - s_{th} = 0. \tag{11}$$

The total noise at the discriminator input consists of three parts, the shot noise from the constant background illumination, the thermal noise of the preamplifier, and the shot noise due to the received signal. The one sided noise current spectral density at the input of the preamplifier can be written as[2]

$$N_n(t) = 2G^2 F \lambda_b + N_{amp} + 2G^2 F s(t), \qquad (A^2/Hz) \tag{12}$$

where $\lambda_b$ is the constant photoelectron rate due to background illumination, $N_{amp}$ is the preamplifier noise current density, and $F$ is the APD excess noise factor. The total noise variance can be written as

$$\sigma_n^2(t) = \frac{1}{2} N_n(t) \tau_n \tag{13}$$

The standard deviation of the ranging error can be obtained by first calculating the threshold level, $s_{th}$, as in Appendix B, solving (11) for the average threshold crossing time, $T_R$, substituting it and (8) and (13) into (4), and then substituting (4) into (1).

## 3. Half Pulse Width Detection

The pulse arrival time in this case is defined as $(t_R+t_F)/2$ with $t_R$ and $t_F$ the threshold crossing times at the leading and trailing edges. The standard deviation of the ranging error in this case is given by

$$\sigma_r = \frac{2}{c} \cdot \frac{\sqrt{\sigma_t^2(T_R) + \sigma_t^2(T_F)}}{2} = \frac{1}{c} \sqrt{\frac{\sigma_n^2(T_R)}{[s'(T_R)]^2} + \frac{\sigma_n^2(T_F)}{[s'(T_F)]^2}} \tag{14}$$

where $T_R$ and $T_F$ are the average threshold crossing times at the leading and trailing edges and they can be obtained by solving (11). Compared with (1), the rms jitter for half pulse width detection is

---

[2] R. G. Smith and S. D. Personick, "Receiver design for optical fiber communication systems," in *Semiconductor Devices for Optical Communication*, Spring-Verlag, New York, 1980, ch. 4.

improved by $1/\sqrt{2}$ over the lead edge detection when the jitters at the rising and trailing edges are equal. The noise variances, $\sigma_n(T_R)$ and $\sigma_n(T_R)$, and slopes, $s'(T_R)$ and $s'(T_F)$ can be obtained by substituting $T_R$ and $T_F$ into (13) and (8).

## 4. Pulse Centroid Detection

The detected pulse arrival time using centroid detection is the same as that of the half pulse width detection provided the received pulse shapes are symmetric. The standard deviation of the ranging error for centroid detection is given by[3]

$$\sigma_r = \frac{2}{c}\sqrt{\frac{F}{\bar{n}}\sigma_L^2 + \frac{1}{\bar{n}^2}\frac{T^2}{12}\left(F\lambda_b T + \frac{N_{th}}{2G^2q^2}T\right)} \tag{15}$$

where $T$ is the observation time, $N_{th}$ ($A^2/Hz$) is the one sided input noise current spectral density of the preamplifier, and $q$ is the electron charge. We used $T=T_{FWHM}$ in the subsequent numerical calculation. In theory, there should be an optimal value for $T$ which minimized the effect of the background and thermal noise and best preserve the received pulse shape. We will study this issue in greater detail in the near future.

## 5. Numerical Calculations and Discussions

Appendix C shows a Mathcad™ program for numerical calculation of the ranging error versus received pulse width and amplitude using MOLA parameter values as an example. The results are presented in Figures 1 through 4.

Figure 1 shows a plot of measurement bias as a function of the received pulse energy (amplitude square) for a 60ns FWHM pulse width and a 5.54 MHz lowpass filter bandwidth. The measurement bias of the leading edge detection decreases as the pulse energy increases. In theory, this bias may be corrected if one also monitors the received pulse energy. The measurement bias for half pulse width detection is

---

[3] C. S. Gardner, "Ranging performance of satellite laser altimeters," *IEEE Trans. Geoscience and Remote Sensing*, Vol. 30, No. 5, pp. 1061-1072, Sept. 1992

almost constant, which equals to the lowpass filter propagation delay and can always be calibrated out. Note we have assumed the received pulse shape is Gaussian and centered at $t=0$. Because the impulse response of the 5 pole lowpass filter is not perfectly symmetric, there is still a slight increase in the bias over pulse energy for half pulse width detection as shown in Figure 1.

Figure 2 shows a plot of measurement bias vs. received FWHM pulse width under constant received pulse energy and the same lowpass filter bandwidth. The half pulse width detection again gives a nearly constant measurement bias, which can be calibrated out once the lowpass filter propagation delay is known. On the other hand, the measurement bias vs. pulse width for leading edge detection first decreases because the pulse gets wider and then increases because the peak of the pulse approaches the threshold level. The rms jitter (error bars) also increases with the pulse width for both of the detection schemes.

Figure 3 shows the standard deviation of the ranging error in nanoseconds vs. the received pulse energy for leading edge, half pulse width, and centroid detections. As expected, the half pulse width detection gives a lower rms jitter than the leading edge detection and the centroid detection always gives the smallest jitter. However, the rate of decrease of the rms jitter becomes slower and slower for the leading edge and half pulse width detections because the slopes of the signal at threshold crossings become shallower and shallower under a constant threshold level.

Figure 4 shows the standard deviation of the ranging error as a function the received pulse width under constant pulse energy. The rms jitters increase very rapidly for relatively large pulse width as the threshold gets close to the peak pulse amplitude where the slope is shallow. There is a moderate improvement in the standard deviation of the ranging error by using centroid detection.

Fig. 1

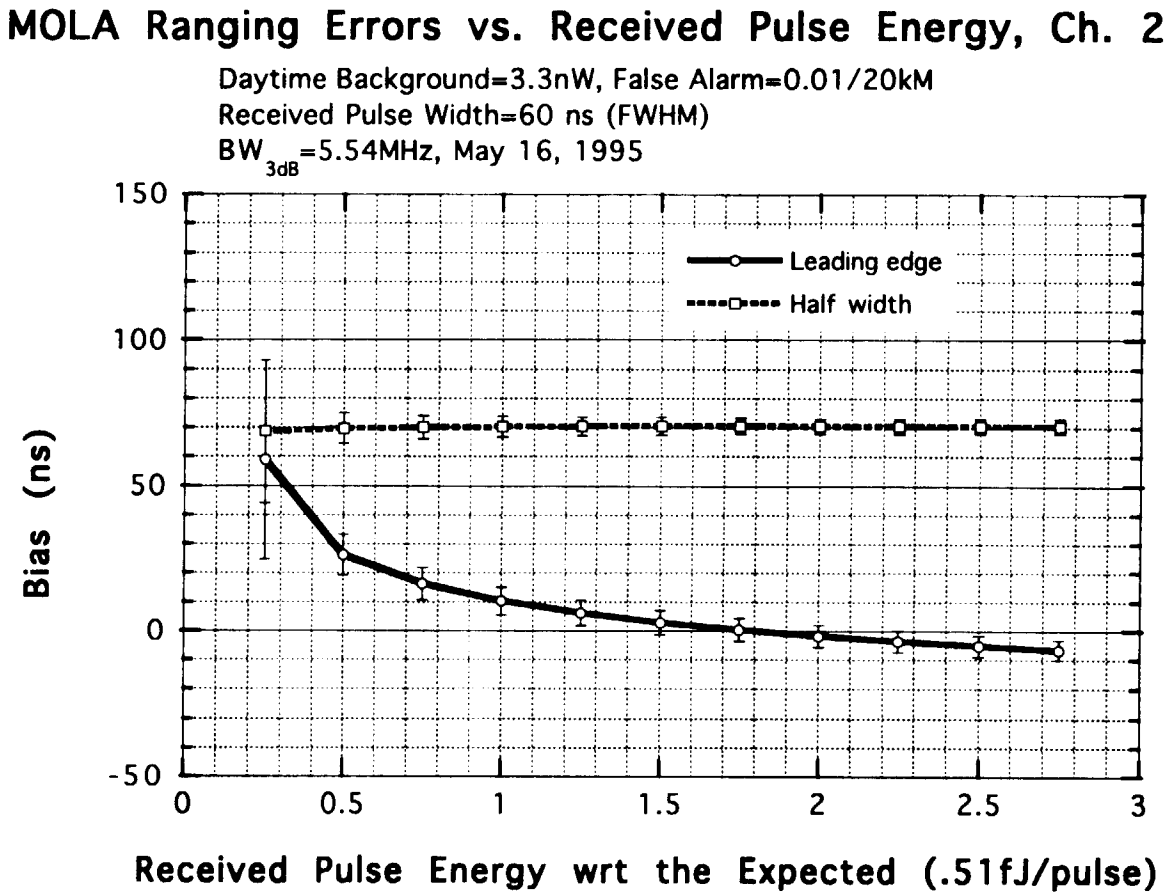
MOLA Ranging Errors vs. Received Pulse Energy, Ch. 2
Daytime Background=3.3nW, False Alarm=0.01/20kM
Received Pulse Width=60 ns (FWHM)
BW3dB=5.54MHz, May 16, 1995
Leading edge
Half width
Bias (ns)
150
100
50
0
-50
0
0.5
1
1.5
2
2.5
3
Received Pulse Energy wrt the Expected (.51fJ/pulse)

Fig. 2

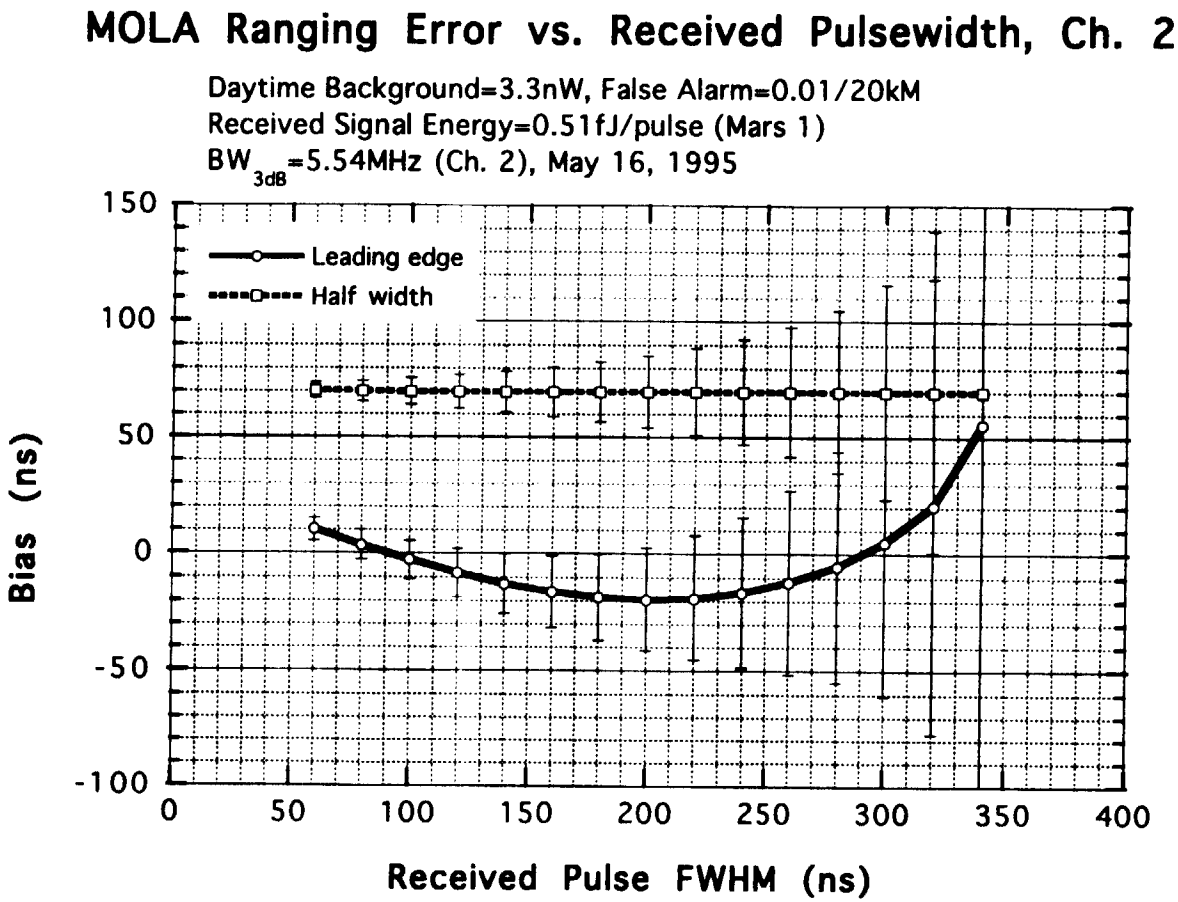
MOLA Ranging Error vs. Received Pulsewidth, Ch. 2
Daytime Background=3.3nW, False Alarm=0.01/20kM
Received Signal Energy=0.51fJ/pulse (Mars 1)
BW3dB=5.54MHz (Ch. 2), May 16, 1995
Leading edge
Half width
Bias (ns)
150
100
50
0
-50
-100
0
50
100
150
200
250
300
350
400
Received Pulse FWHM (ns)

Fig. 3

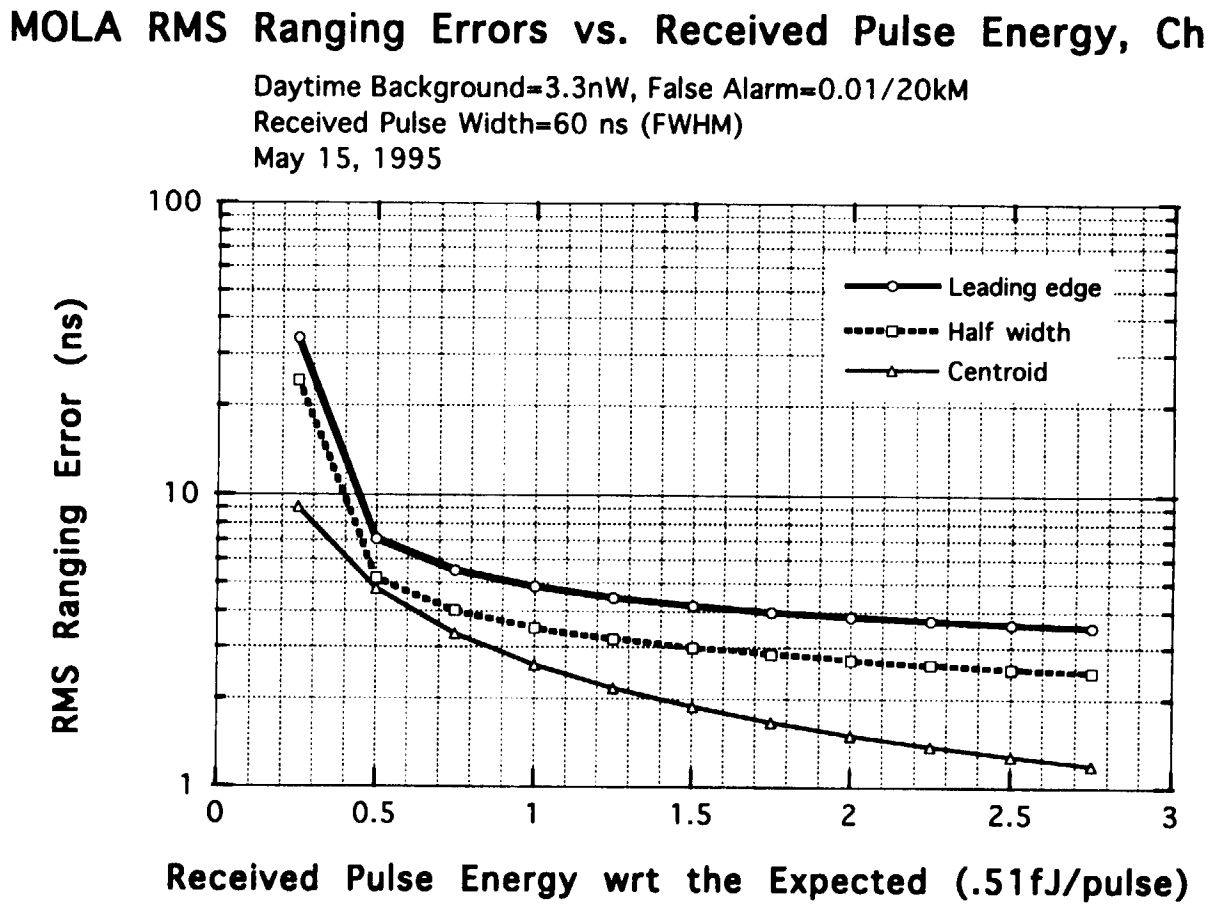
MOLA RMS Ranging Errors vs. Received Pulse Energy, Ch. 2
Daytime Background=3.3nW, False Alarm=0.01/20kM
Received Pulse Width=60 ns (FWHM)
May 15, 1995
RMS Ranging Error (ns)
100
10
1
0
0.5
1
1.5
2
2.5
3
Leading edge
Half width
Centroid
Received Pulse Energy wrt the Expected (.51fJ/pulse)

Fig. 4

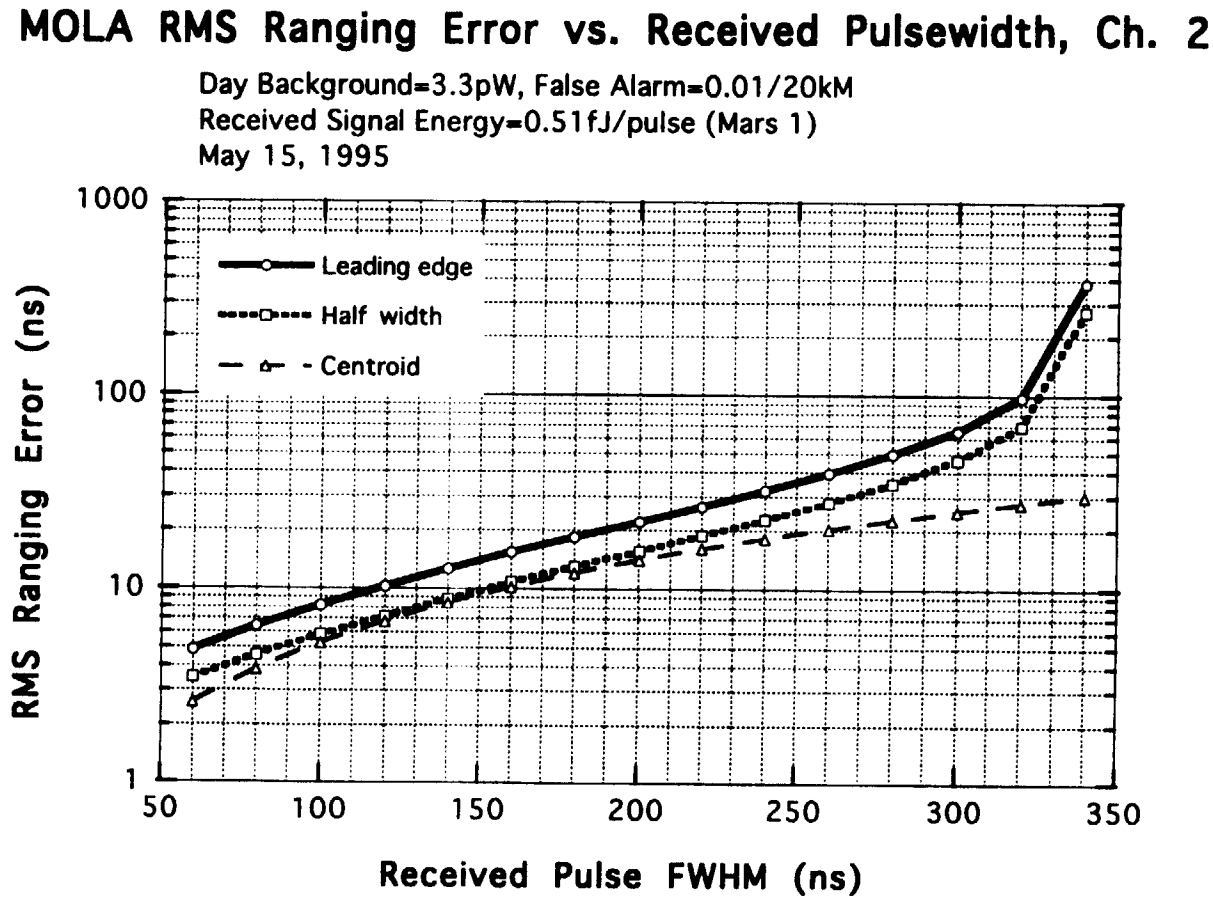
MOLA RMS Ranging Error vs. Received Pulsewidth, Ch. 2
Day Background=3.3pW, False Alarm=0.01/20kM
Received Signal Energy=0.51fJ/pulse (Mars 1)
May 15, 1995
Leading edge
Half width
Centroid
RMS Ranging Error (ns)
1000
100
10
1
50
100
150
200
250
300
350
Received Pulse FWHM (ns)

# Appendix A. Impulse Responses of Fifth Order Bessel Lowpass Filters

Xiaoli Sun/JHU, May 9, 1995

Pole locations: (De Verl S. Humphergs, The Analysis, Design, and Synthesis of Electrical Filters, Prentice-Hall, 1970, p. 421)

$k := 1..5$

$s_1 := -0.9576766 + 1.4711244j$ $\quad$ $s_2 := -0.9576766 - 1.4711244j$

$s_3 := -1.3808774 + 0.7179096j$ $\quad$ $s_4 := -1.3808774 - 0.7179096j$

$s_5 := -1.5023160$

Multiplication factor (such that H0)=0)

$$a0 := \left(\prod_k \frac{1}{-s_k}\right)^{-1} \qquad a0 = 11.2128369$$

Coefficients of partial fractions

$s1 := s_1$

$$A_1 := \frac{a0}{(s1 - s_2)\cdot(s1 - s_3)\cdot(s1 - s_4)\cdot(s1 - s_5)} \qquad A_1 = 0.6193646 + 1.0986249j$$

$s1 := s_2$

$$A_2 := \frac{a0}{(s1 - s_1)\cdot(s1 - s_3)\cdot(s1 - s_4)\cdot(s1 - s_5)} \qquad A_2 = 0.6193646 - 1.0986249j$$

$s1 := s_3$

$$A_3 := \frac{a0}{(s1 - s_1)\cdot(s1 - s_2)\cdot(s1 - s_4)\cdot(s1 - s_5)} \qquad A_3 = -4.916811 - 2.6131065j$$

$s1 := s_4$

$$A_4 := \frac{a0}{(s1 - s_1)\cdot(s1 - s_2)\cdot(s1 - s_3)\cdot(s1 - s_5)} \qquad A_4 = -4.916811 + 2.6131065j$$

$s1 := s_5$

$$A_5 := \frac{a0}{(s1 - s_1)\cdot(s1 - s_2)\cdot(s1 - s_3)\cdot(s1 - s_4)} \qquad A_5 = 8.5948928$$

The Impulse Response Function

$$hh(t, BW_{3dB}) := \left[\sum_k A_k \cdot \exp(s_k \cdot (2\cdot\pi\cdot BW_{3dB})\cdot t)\right]\cdot 2\cdot\pi\cdot BW_{3dB}$$

The real impulse response function:

$$h(t, BW_{3dB}) := Re(hh(t, BW_{3dB}))$$

Note the imaginary part
is not canceled out completely
due to computer quantization error.

Numerical results of the normalized filter

$$BW_{3dB} := \frac{1}{2\cdot\pi}\cdot\frac{1}{sec} \qquad \text{(1 rad/sec)}$$

$$k := 0..500 \qquad t0_k := 0.02\cdot k\cdot sec$$

$$h0_k := h(t0_k, BW_{3dB})$$

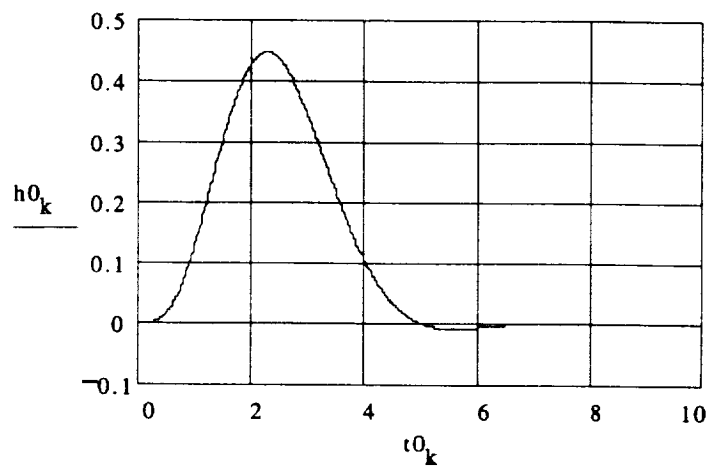


FWHM pulsewidth:

$t1 := 1\cdot sec$ Initial guess

$$T1 := root(linterp(t0, h0, t1) - 0.5\cdot max(h0), t1)$$

$t2 := 3\cdot sec$

$$T2 := root(linterp(t0, h0, t2) - 0.5\cdot max(h0), t2)$$

$W0 := T2 - T1 \qquad W0 = 2.204\cdot sec$

The actual pulse width:

$$T_{FWHM}(BW_{3dB}) := \frac{W0}{2\cdot\pi\cdot BW_{3dB}}$$

e.g., for MOLA 20 ns filter (3dB bandwidth=16.6MHz),

$$T_{FWHM}(16.6\cdot 10^6) = 2.113\cdot 10^{-8}\cdot sec$$

One sided noise bandwidth:

$$BW_n := \frac{1}{2}\cdot\int_{0\cdot sec}^{100\cdot sec} h(t, BW_{3dB})^2\, dt \qquad \frac{BW_n}{BW_{3dB}} = 1.039$$

# Appendix B. Calculation of MOLA Discriminator Threshold Level

Xiaoli Sun/JHU, May 9, 1995

Average # of background radiation photons/s

$I_{solar} := 0.311 \cdot 1$ Solar irradiance at the target (W/m^2/nm)

$r_{diff} := 0.26$ Target diffusion coefficient

$\phi_{tel} := 0.508$ Receiver Telescope Diameter (m)

$\eta_{obs} := .19$ Telescope obscuration ratio

$\theta_{FOV} := 0.847 \cdot 10^{-3}$ Receiver FOV (rad)

$\eta_{rcvr} := 0.63$ Receiver optics transmission

$\eta_{atmo} := 0.5$ Atmosphere Transmission Coefficient (one way)

$\eta_{APD} := 0.3$ APD quantum efficiency

$\Delta\lambda := 2.2$ Receiver optical bandwidth (nm)

$R := 410 \cdot 10^{3}$ Orbit altitude (m)

$I_b := 50 \cdot 10^{-12}$ APD bulk leakage current (A)

Background noise power

$$P_b := I_{solar} \cdot \Delta\lambda \cdot \eta_{rcvr} \cdot \pi \cdot \left(\frac{\theta_{FOV} \cdot R}{2}\right)^2 \cdot \frac{r_{diff}}{\pi} \cdot \frac{\pi \cdot \frac{\phi_{tel}^2}{4} \cdot (1 - \eta_{obs})}{R^2} \qquad P_b = 3.3 \cdot 10^{-9}$$

$$\lambda_b := \frac{\eta_{APD} \cdot P_b}{1.17 \cdot 1.6 \cdot 10^{-19}} + \frac{I_b}{1.6 \cdot 10^{-19}} \qquad \lambda_b = 5.6 \cdot 10^{9}$$

$$\frac{I_b}{1.6 \cdot 10^{-19}} = 3.1 \cdot 10^{8}$$

APD Spectral Noise Density

$G := 120$ Average APD gain

$k_{eff} := 0.007$ APD ionization coefficient ratio

$F := G \cdot k_{eff} + \left(2 - \frac{1}{G}\right) \cdot (1 - k_{eff})$ APD excess noise factor $F = 2.82$

$N_{APD} := 2 \cdot G^2 \cdot F \cdot \lambda_b$ APD noise current density (A^2/Hz) normalized wrt q

Preamplifier Thermal Noise Spectral Density:

$N_V := \frac{(195 \cdot 10^{-6})^2}{24 \cdot 10^6}$ Preamp dark noise density given by EG&G (V^2/Hz)

$R_l := 20000$ APD load resistance (ohm)

Equivalent noise current at input (A/Hz^1/2) $\frac{\sqrt{N_V}}{R_l} = 1.99 \cdot 10^{-12}$

$N_{amp} := \frac{N_V}{R_l^2 \cdot (1.6 \cdot 10^{-19})^2}$ Equivalent noise current density normalized wrt q

Noise due to APD surface leakage current:

$I_s := 15 \cdot 10^{-9}$ APD surface leakage current (A) $N_{Is} := 2 \cdot \frac{I_s}{1.6 \cdot 10^{-19}}$

Other system parameter values:

$R_G := 20$ Range gate (km)

$T := 2 \cdot \frac{R_G \cdot 1000}{3 \cdot 10^8}$ Range gate interval (sec) $T = 1.33 \cdot 10^{-4}$

Matched Filter Noise Bandwidth (5 pole Bessel LPF)

$BW_{3dB} := 5.54 \cdot 10^6$ (Channel 2)

$BW_n := 1.039 \cdot BW_{3dB}$ (see Appendix A)

$\tau := \frac{1}{2 \cdot BW_n}$ equivalent integration time for noise photons $\tau = 8.69 \cdot 10^{-8}$

Equivalent average # of noise photoelectrons:

$\mu_0 := \frac{N_{APD} \cdot BW_n \cdot \tau^2}{G^2 \cdot F}$ $\mu_0 = 4.87 \cdot 10^2$

The variance of the preamplifier noise and APD surface leakage current noise (Gaussian):

$var := (N_{amp} + N_{Is}) \cdot BW_n \cdot \tau^2$

$\sigma := \sqrt{var}$ $\sigma = 2.59 \cdot 10^3$ $\frac{\sigma}{G} = 2.16 \cdot 10^1$

The p.d.f. of the APD output:

$$s_{00} := \sqrt{G^2 \cdot F \cdot \mu_0} \qquad s_{00} = 4.44 \cdot 10^3$$

$$P_{PD0}(z) := \frac{1}{\sqrt{2 \cdot \pi}} \cdot \frac{1}{\left[1 + \frac{G \cdot (F-1) \cdot z}{s_{00}}\right]^{\frac{3}{2}}} \cdot \exp\left[\frac{-z^2}{2 \cdot \left[1 + \frac{G \cdot (F-1) \cdot z}{s_{00}}\right]}\right]$$

(see the attached notes for the derivation of the above equation)

Probabilities of false alarm:

$$s_0 := \sqrt{s_{00}^2 + \sigma^2} \qquad s_0 = 5.14 \cdot 10^3$$ Standard deviation of the total noise

$$z_0 := \frac{-G \cdot \mu_0}{s_{00}} \qquad z_0 = -1.31 \cdot 10^1$$ lower limit of the integral

$$z_1 := 30$$ Upper limit of the integral

$$p_{fa}(n_T) := \int_{z_0}^{z_1} P_{PD0}(z) \cdot \mathrm{cnorm}\left(\frac{s_{00} \cdot z - n_T \cdot s_0}{\sigma}\right) dz$$

(see the attached notes for derivation)

The built-in function "cnorm(u)" is the culmulative probability distribution function of a Gaussian r.v. with zero mean and unity variance

$$P_{FA}(n_T) := 1 - \exp(-T \cdot BW_{3dB} \cdot p_{fa}(n_T))$$

Assuming the average pulsewidth is 1/BW.

$M := 10$

$k := 0, 1 .. M$

$NT_k := 3 + 0.2 \cdot k$ Normalized threshold level

$TOL := 10^{-12}$ The integration error tolerance

$pfa_k := p_{fa}(NT_k)$

$PFA_k := 1 - \exp(-T \cdot BW_{3dB} \cdot pfa_k)$

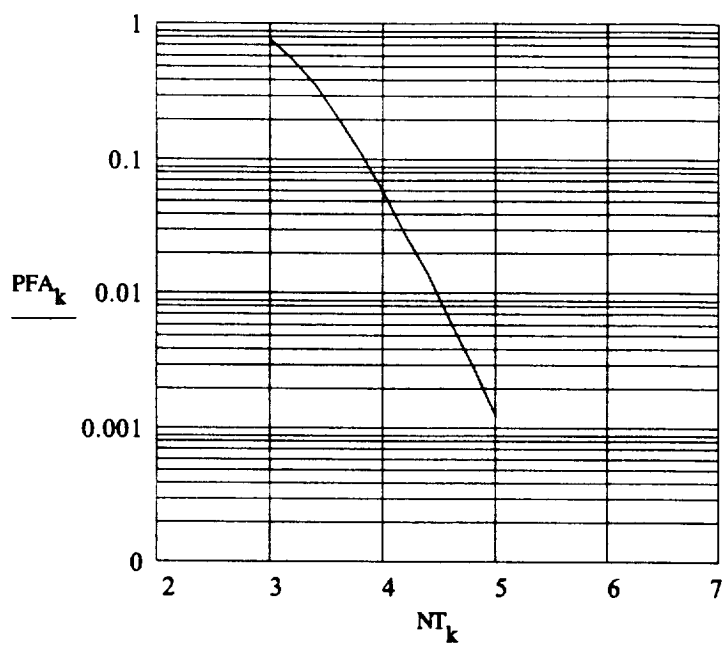


Normalized Threshold level at PFA=0.01:

$PPFA_k := PFA_{M-k}$ $NNT_k := NT_{M-k}$

$Thre := linterp(PPFA, NNT, 0.01)$

$Thre = 4.5$ for $BW_{3dB} = 5.54 \cdot 10^6$

$s_0 = 5.14 \cdot 10^3$

## Notes to Appendix B:

The average rate of false alarms can be calculated as[1]

$$T_{FA}^{-1}=\frac{p_{fa}}{\tau_W} \tag{1}$$

where $p_{fa}$ is the false alarm probability at a fixed time and $\tau_W$ is the average noise pulse width above the threshold. It may be assumed that $\tau_W=1/BW_{3dB}$. The number of false alarms over a given range gate time, $T_G$, follows a Poisson distribution and the false alarm probability is given by

$$P_{FA}=1-\exp\left[-\frac{T_G}{T_{FA}}\right]=1-\exp[-T_G BW_{3dB} p_{fa}] \tag{2}$$

The false alarm probability at a fixed time can be written as

$$p_{fa}=\int_{y_T}^{\infty} p(y|\mu_0)dy=\int_{y_T}^{\infty}\int_0^{\infty}\frac{1}{\sqrt{2\pi}\sigma}\exp\left[-\frac{(y-x-\mu_g)^2}{2\sigma^2}\right]P_{PD}(x|\mu_0)dxdy \tag{3}$$

where $p(y|\mu_0)$ is the p.d.f. of the APD preamplifier output and is equal to the convolution of the p.d.f. of the APD output and the p.d.f. of the preamplifier noise. The latter is assumed to be additive and Gaussian with mean, $\mu_g$, and standard deviation, $\sigma$. Usually, the preamplifier itself has zero DC offset, $\mu_g=I_s\tau/q$ with $I_s$ the APD surface leakage current, $\tau$ the equivalent integration time of the lowpass filter, and q the electron charge. The variance is given by

$$\sigma^2=(N_{amp}+2I_s)BW_n\tau^2/q^2 \tag{4}$$

with $N_{amp}$ the one sided input noise spectral density of the preamplifier in ($A^2$/Hz) and $BW_n$ the noise bandwidth of the lowpass filter.

The p.d.f. of the APD output in number of photoelectrons is given by[2]

$$P_{PD}(x|\mu_0)=\frac{1}{\sqrt{2\pi G^2F\mu_0}}\frac{1}{\left[1+\frac{(x-G\mu_0)(F-1)}{GF\mu_0}\right]^{3/2}}\exp\left\{\frac{-(x-G\mu_0)^2}{2G^2F\mu_0\left[1+\frac{(x-G\mu_0)(F-1)}{GF\mu_0}\right]}\right\} \tag{5}$$

---

[1] M. I. Skolnik, Introduction to Radar Systems, McGraw-Hill, New York, 1962, p. 31.
[2] P. P. Webb, R. J. McIntyre, and J. Conradi, "Property of avalanche photodiodes," *RCA Review*, Vol. 35, pp. 234-278, June 1974.

where $\mu_0$ is the average number of primary photoelectrons given by

$$\mu_0=\frac{\eta_{APD}P_b\tau}{hf}+\frac{I_b\tau}{q} \tag{6}$$

with $\eta_{APD}$ the APD quantum efficiency, $P_b$ the received background noise power, hf the photon energy, and $I_b$ the APD bulk leakage current.

Interchange the order of integration in Eq. (3) and substitute $u=(x-y)/\sigma$, and $z=(x-G\mu_0)/(G^2F\mu_0)^{1/2}$ ,

$$p_{fa}=\int_0^{\infty}\left\{\int_{y_T}^{\infty}\frac{1}{\sqrt{2\pi}\sigma}\exp\left[-\frac{(y-x-\mu_g)^2}{2\sigma^2}\right]dy\right\}P_{PD}(x|\mu_0)dx$$

$$=\int_0^{\infty}\left\{\int_{-\infty}^{\frac{x-y_T+\mu_g}{\sigma}}\frac{1}{\sqrt{2\pi}}\exp\left[-\frac{u^2}{2}\right]du\right\}P_{PD}(x|\mu_0)dx$$

$$=\int_{\frac{-G\mu_0}{\sqrt{G^2F\mu_0}}}^{\infty}\Phi\left[\frac{\sqrt{G^2F\mu_0}\,z-(y_T-G\mu_0-\mu_g)}{\sigma}\right]P_{PDZ}(z|\mu_0)dz \tag{7}$$

$$\Phi[x]=\int_{-\infty}^{x}\frac{1}{\sqrt{2\pi}}\exp\left[-\frac{u^2}{2}\right]du \tag{8}$$

$$P_{PDZ}(z|\mu_0)=\frac{1}{\sqrt{2\pi}}\frac{1}{\left[1+\frac{G(F-1)z}{\sqrt{G^2F\mu_0}}\right]^{3/2}}\exp\left\{\frac{-z^2}{2\left[1+\frac{G(F-1)z}{\sqrt{G^2F\mu_0}}\right]}\right\} \tag{9}$$

A normalized threshold is defined as

$$Y_T=\frac{y_T-(G\mu_0+\mu_g)}{\sqrt{G^2F\mu_0+\sigma^2}} \tag{10}$$

that is, the actual threshold is $Y_T$ times the total noise standard deviation plus the average DC component of the APD output. Usually, $\mu_g<<G\mu_0$, we can drop $\mu_g$ in the calculations.

# Appendix C. Calculation of Ranging Errors of MOLA vs. Pulse Width and Amplitude for Leading Edge, Half Width, and Centroid Detections

Xiaoli Sun/Code 924/JHU, May 11, 1995

System parameters

Received laser pulse energy $E_r := .510 \cdot 10^{-15} \cdot joule$

APD quantum efficiency $\eta := .30$

Average # photoelectrons/pulse $n_{bar} := \frac{E_r \cdot \eta}{(1.17 \cdot 1.6 \cdot 10^{-19}) \cdot joule}$ $n_{bar} = 817$

Received pulse width (FWHM) $T_{FWHM} := 60 \cdot 10^{-9} \cdot sec$

Matched Filter 3dB BW $BW_{LPF} := 5.54 \cdot 10^{6} \cdot Hz$ $Hz \equiv \frac{1}{sec}$

Average APD gain $G := 120$

APD ionization coefficient ratio $k_{eff} := 0.007$

APD surface leakage current $I_s := 15 \cdot 10^{-9} \cdot amp$

APD bulk leakage current $I_b := 50 \cdot 10^{-12} \cdot amp$

Preamp input noise current density $N_a := \left(\frac{2 \cdot 10^{-12}}{1.6 \cdot 10^{-19}}\right)^2 \cdot \frac{1}{sec}$

Backgound illumination power into the APD $P_b := 3.3 \cdot 10^{-9} \cdot watt$

Noise and threshold levels (copied from Appendix B for Ch. 1):

$s_0 := 5.14 \cdot 10^3$ Standard deviation of the APD and preamp noises

$Thre := 4.50$ Normalized threshold for PFA=0.01 per range gate daytime

$\tau_n := \frac{1}{2 \cdot 1.039 \cdot BW_{LPF}}$ Equivalent noise integration time of the lowpass filter

Background photoelectron rate: $\lambda_b := \frac{\eta \cdot P_b}{1.17 \cdot 1.6 \cdot 10^{-19} \cdot joule} + \frac{I_b}{1.6 \cdot 10^{-19} \cdot coul}$

Total additive Gaussian noise density: $N_{amp} := N_a + \frac{2 \cdot I_s}{1.6 \cdot 10^{-19} \cdot coul}$

Laser pulse shape function:

RMS pulse width $\sigma_L(T_{FWHM}) := \frac{T_{FWHM}}{2 \cdot \sqrt{2 \cdot \ln(2)}}$ $\sigma_L(T_{FWHM}) = 2.548 \cdot 10^{-8} \cdot sec$

Laser pulse shape $p(t, T_{FWHM}) := \frac{1}{\sqrt{2 \cdot \pi} \cdot \sigma_L(T_{FWHM})} \cdot \exp\left(-\frac{t^2}{2 \cdot \sigma_L(T_{FWHM})^2}\right)$

Impulse Response of the lowpass filters:

5th order Bessel LPF

Pole locations $k := 1..5$

$s_1 := -0.9576766 + 1.4711244j$ $\quad s_2 := -0.9576766 - 1.4711244j$

$s_3 := -1.3808774 + 0.7179096j$ $\quad s_4 := -1.3808774 - 0.7179096j$

$s_5 := -1.5023160$

Coefficients of partial fractions

$A_1 := 0.6193646 + 1.0986249j$ $\quad A_2 := 0.6193646 - 1.0986249j$

$A_3 := -4.916811 - 2.6131065j$ $\quad A_4 := -4.916811 + 2.6131065j$

$A_5 := 8.5948928$

Impulse Response:

$$h(t) := \mathrm{Re}\left[\left[\sum_k A_k \cdot \exp(s_k \cdot (2 \cdot \pi \cdot BW_{LPF}) \cdot t)\right] \cdot 2 \cdot \pi \cdot BW_{LPF}\right]$$

Average signal (secondary photoelectrons per $\tau$ second):

$$s(t, n_{bar}, T_{FWHM}) := n_{bar} \cdot G \cdot \tau_n \cdot \int_{-5 \cdot \sigma_L(T_{FWHM})}^{t} p(u, T_{FWHM}) \cdot h(t-u)\, du$$

Total noise variance calculation:

APD excess noise factor $\quad F := k_{eff} \cdot G + \left(2 - \frac{1}{G}\right) \cdot (1 - k_{eff})$

$$var_1(t, n_{bar}, T_{FWHM}) := F \cdot G^2 \cdot n_{bar} \cdot \tau_n^2 \cdot \int_{-5 \cdot \sigma_L(T_{FWHM})}^{t} p(\tau, T_{FWHM}) \cdot h(t-\tau)^2\, d\tau$$

$$var(t, n_{bar}, T_{FWHM}) := var_1(t, n_{bar}, T_{FWHM}) + s_0^2$$

Derivative of the signal:

$$dpdt(t, T_{FWHM}) := -\frac{t}{\sigma_L(T_{FWHM})^2} \cdot p(t, T_{FWHM})$$

$$dsdt(t, n_{bar}, T_{FWHM}) := n_{bar} \cdot G \cdot \tau_n \cdot \int_{-5 \cdot \sigma_L(T_{FWHM})}^{t} dpdt(u, T_{FWHM}) \cdot h(t-u)\, du$$

Example (ATU signal laser):

$i := 0..38 \qquad t_i := (i)\cdot 0.05\cdot(\tau_n + T_{FWHM}) - 1.0\cdot T_{FWHM}$

$S_i := s(t_i, n_{bar}, T_{FWHM}) \qquad THRE_i := Thre\cdot s_0$

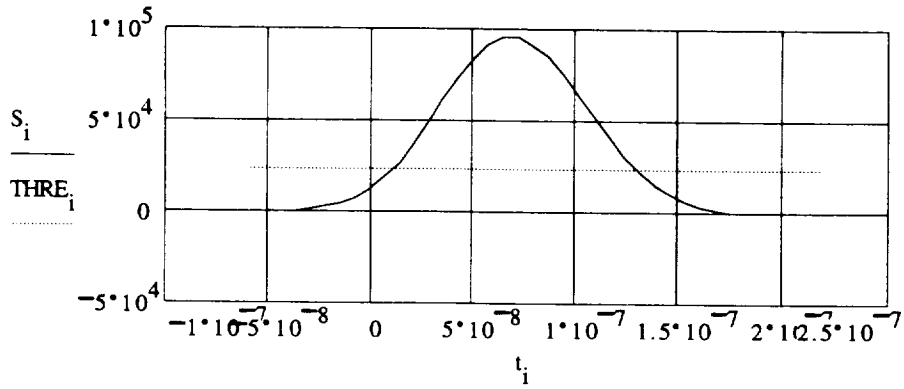


Solve for the threshold crossing times

equation to solve $\quad f(T_{FWHM}, n_{bar}, t1) := root(s(t1\cdot sec, n_{bar}, T_{FWHM}) - Thre\cdot s_0, t1)$

Rising edge:

$t1 := -0.3\cdot T_{FWHM}\cdot\frac{1}{sec}$ initial guess

$TR := f(T_{FWHM}, n_{bar}, t1) \qquad TR = 1.03\cdot 10^{-8}$

Falling edge:

$t2 := (0.5\cdot T_{FWHM} + \tau_n)\cdot\frac{1}{sec}$

$TF := f(T_{FWHM}, n_{bar}, t2) \qquad TF = 1.303\cdot 10^{-7}$

Half width location:

$TH := \frac{TF + TR}{2} \qquad TH = 7.029\cdot 10^{-8}$

RMS jitter at threshold crossing:

$$\sigma_{\tau r} := \sqrt{\frac{var(TR\cdot sec, n_{bar}, T_{FWHM})}{dsdt(TR\cdot sec, n_{bar}, T_{FWHM})^2}} \qquad \sigma_{\tau f} := \sqrt{\frac{var(TF\cdot sec, n_{bar}, T_{FWHM})}{dsdt(TF\cdot sec, n_{bar}, T_{FWHM})^2}}$$

$$\sigma_{\tau h} := 0.5\cdot\sqrt{\sigma_{\tau r}^2 + \sigma_{\tau f}^2}$$

$$\sigma_{\tau c} := \sqrt{\frac{F}{n_{bar}}\cdot\sigma_L(T_{FWHM})^2 + \frac{1}{n_{bar}^2}\cdot\frac{(2\cdot T_{FWHM})^3}{12}\cdot\left(F\cdot\lambda_b + \frac{N_{amp}}{2\cdot G^2}\right)}$$

$\sigma_{\tau r} = 4.836\cdot 10^{-9}\cdot sec \qquad \sigma_{\tau h} = 3.507\cdot 10^{-9}\cdot sec \qquad \sigma_{\tau c} = 2.61\cdot 10^{-9}\cdot sec$

NUMERICAL CALCULATION -- Ranging error vs. pulse energy:

Received Photons/pulse:

$i := 0..10$ $\qquad$ $nbar_i := (i \cdot 0.25 + 0.25) \cdot n_{bar}$

Solve for the threshold crossing times

equation to solve

$$f(T_{FWHM}, n_{bar}, t1) := root(s(t1 \cdot sec, n_{bar}, T_{FWHM}) - Thre \cdot s_0, t1)$$

Rising edge: $\quad t1_i := -\left[-T_{FWHM} + \tau_n \cdot \left(1 - \frac{nbar_i}{n_{bar}}\right)\right] \cdot 0.2 \cdot \frac{1}{sec}$ $\quad$ initial guess

$$TR_i := f(T_{FWHM}, nbar_i, t1_i)$$

Falling edge: $\quad t2 := (0.5 \cdot T_{FWHM} + \tau_n) \cdot \frac{1}{sec}$ $\quad$ initial guess

$$TF_i := f(T_{FWHM}, nbar_i, t2)$$

Average (half width):

$$TH_i := 0.5 \cdot (TR_i + TF_i)$$

RMS jitter at threshold crossing:

$$\sigma r_i := \sqrt{\frac{var(TR_i \cdot sec, nbar_i, T_{FWHM})}{dsdt(TR_i \cdot sec, nbar_i, T_{FWHM})^2}} \qquad \sigma f_i := \sqrt{\frac{var(TF_i \cdot sec, nbar_i, T_{FWHM})}{dsdt(TF_i \cdot sec, nbar_i, T_{FWHM})^2}}$$

$$\sigma h_i := \frac{1}{2} \cdot \sqrt{(\sigma r_i)^2 + (\sigma f_i)^2}$$

$$\sigma c_i := \sqrt{\frac{F}{nbar_i} \cdot \sigma_L(T_{FWHM})^2 + \frac{1}{(nbar_i)^2} \cdot \frac{(2 \cdot T_{FWHM})^3}{12} \cdot \left(F \cdot \lambda_b + \frac{N_{amp}}{2 \cdot G^2}\right)}$$

The Results:

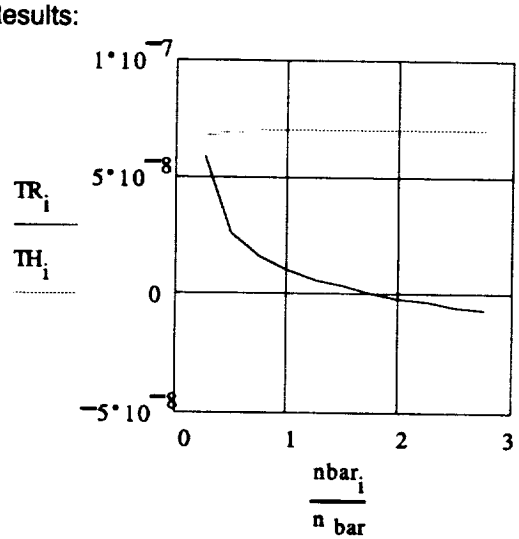


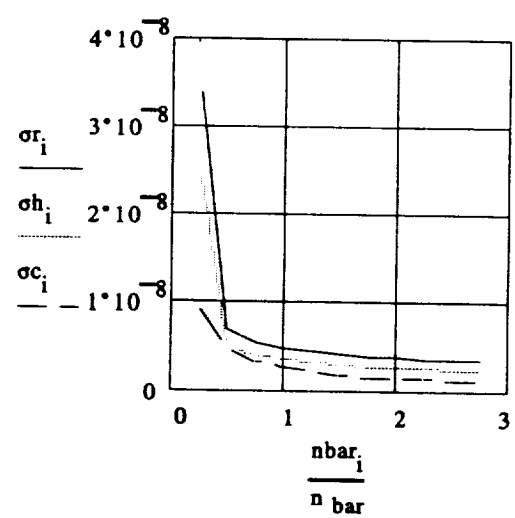


$$WRITEPRN(TXvsNbar) := augment\left(\frac{nbar}{n_{bar}}, augment\left(TR, augment\left(TH, augment\left(\frac{\sigma r}{sec}, augment\left(\frac{\sigma h}{sec}, \frac{\sigma c}{sec}\right)\right)\right)\right)\right)$$

NUMERICAL CALCULATION -- Ranging error vs. pulse width:

Received pulse width: $i := 0..14$ $\quad TFWHM_i := (i \cdot 20 \cdot 10^{-9} + 60 \cdot 10^{-9}) \cdot sec$

Solve for the threshold crossing times

equation to solve

$$f(T_{FWHM}, n_{bar}, t1) := root(s(t1 \cdot sec, n_{bar}, T_{FWHM}) - Thre \cdot s_0, t1)$$

Rising edge: $t1_i := (-0.5 \cdot TFWHM_i + \tau_n) \cdot \frac{1}{sec}$ initial guess

$$TR_i := f(TFWHM_i, n_{bar}, t1_i)$$

Falling edge: $t2_i := (0.5 \cdot TFWHM_i + \tau_n) \cdot \frac{1}{sec}$ initial guess

$$TF_i := f(TFWHM_i, n_{bar}, t2_i)$$

Average (half width): $TH_i := 0.5 \cdot (TR_i + TF_i)$

RMS jitter at threshold crossing:

$$\sigma r_i := \sqrt{\frac{var(TR_i \cdot sec, n_{bar}, TFWHM_i)}{dsdt(TR_i \cdot sec, n_{bar}, TFWHM_i)^2}} \qquad \sigma f_i := \sqrt{\frac{var(TF_i \cdot sec, n_{bar}, TFWHM_i)}{dsdt(TF_i \cdot sec, n_{bar}, TFWHM_i)^2}}$$

$$\sigma h_i := \frac{1}{2} \cdot \sqrt{(\sigma r_i)^2 + (\sigma f_i)^2}$$

$$\sigma c_i := \sqrt{\frac{F}{n_{bar}} \cdot \sigma_L(TFWHM_i)^2 + \frac{1}{(n_{bar})^2} \cdot \frac{(2 \cdot TFWHM_i)^3}{12} \cdot \left(F \cdot \lambda_b + \frac{N_{amp}}{2 \cdot G^2}\right)}$$

The Results:

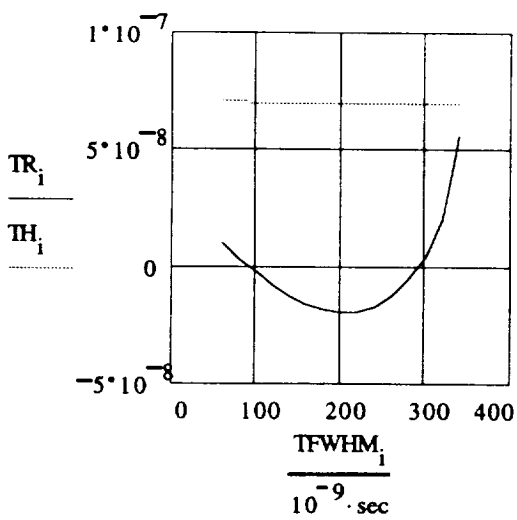


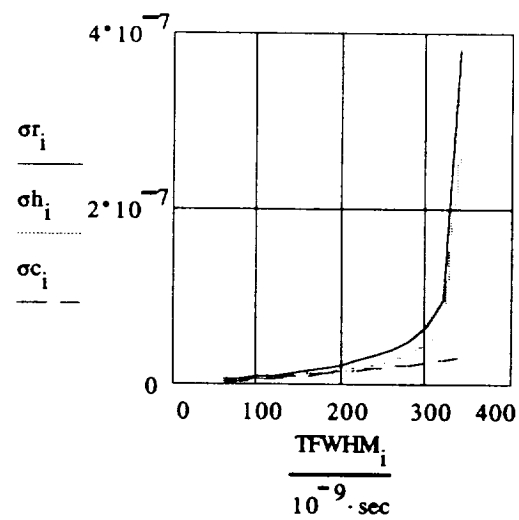


$$WRITEPRN(TXvsW) := augment\left(\frac{TFWHM}{sec}, augment\left(TR, augment\left(TH, augment\left(\frac{\sigma r}{sec}, augment\left(\frac{\sigma h}{sec}, \frac{\sigma c}{sec}\right)\right)\right)\right)\right)$$

# Final Report on GAMES Master Oscillator

Christopher T. Field
Electrical and Computer Engineering
The Johns Hopkins University

May 15, 1995

## 1 Introduction

The Gravity and Magnetic Earth Survey (GAMES) is a mission to measure the Earth's gravity field by recording the relative velocity between a main satellite and a sub-satellite which are in identical orbits. The relative velocity will be measured to about 20 $\mu$m/s when the range is 100 km and 50 $\mu$m/s when the range is 200 km.

There will be three optical ranging signals. A pseudo-random binary sequence at 31.25 Mbits/s. will intensity modulate the tracking laser diodes. A mirror retro-reflector on the sub-satellite returns laser light from the main satellite back to it. Correlation of the received light with the transmitted signal will determine the inter-satellite distance to 4.8 meters. A second laser will be intensity modulated by medium and fine ranging sine waves. The medium signal will also be 31.25 MHz. Resolution of the difference between the transmitted and received phase to 5 degrees will determine the inter-satellite distance to 70 mm with a 4.8 meter range ambiguity. The fine ranging signal, 2 GHz, has a 75 mm range ambiguity. Assuming the ranging frequency is known exactly, determining the transmitted and received phase difference to 0.1 degrees will yield the range to 20 $\mu$m. The phase difference will be reported about 250 times each second. Tracking the phase difference as a function of time will give the inter-satellite relative velocity. Velocity variations are expected to take longer than 10 seconds.

This report describes the system oscillator specification required to meet the performance goals.

The transmitted fine and medium ranging signals may be written as

$$v_T(t) = v_0 \sin(t\omega_c + \phi_0) \tag{1}$$

where $\omega_c$ is the modulation angular frequency and $\phi_0$ is the initial phase. The received signal is an attenuated, time shifted copy of the transmitted signal and can be written as

$$v_R(t) = v_0' \sin((t - \tau_d)\omega_c + \phi_0) \tag{2}$$

where $\tau_d$ is the round trip time delay. Denote the transmitted and received phases by

$$\alpha_T(t) = t\omega_c + \phi_0(t) \tag{3a}$$

$$\alpha_R(t) = (t - \tau_d)\omega_c + \phi_0(t - \tau_d) \tag{3b}$$

where account for oscillator imperfections have been taken by writing a time dependent phase. Multiplying the transmitted and received signals yields a term proportional to the sine of the phase difference

$$\Delta\alpha(t) = \alpha_T(t) - \alpha_R(t) = \tau_d\omega_c + \phi_0(t) - \phi_0(t - \tau_d) \tag{4}$$

The measured phase difference is proportional to the time delay and frequency and also depends on the oscillator phase variations.

Because the phase difference is proportional to the frequency, the accuracy of the fine range measurement depends critically on the stability of the master oscillator. This report summaries the oscillator frequency and phase variations effects on the fine ranging performance. The analysis focuses on the fine ranging system, but the same mathematics governs the medium ranging system.

Measurement of the phase difference, $\Delta\alpha(t)$, could be performed by mixing the transmitted signal with the received signal. While doing so is functionally simple it has the disadvantages that the final output signal is essentially DC and subject to $1/f$ noise, DC drifts, and other measurement errors. In fact the received signal is mixed with a local oscillator offset from the transmitted signal frequency by an intermediate frequency, $\omega_i$. The resultant low frequency signal is digitized so that the final phase determination is immune to $1/f$ noise, DC drifts, offset errors, etc.

The rest of this work is structured as follows. Section 2 summarizes the GAMES oscillator performance requirements. Section 3 describes crystal oscillators and oscillator frequency and phase noise. Methods for expressing oscillator

noise are covered. Also covered is the phase noise power spectrum after taking the difference of oscillator phase taken at different times. Section 4 relates the specification of a few commercially available oscillators to the requirements. The appendix derives the expressions used to determine the oscillator performance requirements. Finally there is a short list of useful references.

# 2 GAMES Oscillator Requirements.

There are three constraints on the oscillator performance. The desired relative velocity resolution limits the permissible rate of frequency change, both deterministic and random. Oscillator phase noise introduces random noise somewhat like amplifier thermal noise. The permitted noise level must be specified. The absolute frequency stability determines the inter-satellite range accuracy.

For GAMES, the relative velocity between the main and sub-satellite must be measured to 20–50$\mu$m/s. So that the oscillator will be an insignificant error source, it will be specified to introduce a velocity error no larger than 1$\mu$m/s and phase noise no greater than the thermal noise contribution of the PMT pre-amplifier. Table 1 defines the symbols used in this work.

The required oscillator specifications may be summarized by

1. A range rate accuracy of $\Delta v$ measured over a time period $\Delta t$ requires two range measurements with a permitted range error of $\Delta r = \Delta t \Delta v/2$. The maximum permitted frequency change is given by $\Delta f_c/f_c \leq \Delta t \Delta v/2r$ or $\Delta f_c/(f_c \Delta t) \leq \Delta v/2r = 2 \times 10^{-12}$/s, $1 \times 10^{-8}$/hour, $2 \times 10^{-7}$/day, $7 \times 10^{-6}$/month, or $7 \times 10^{-5}$/year.

2. So that the phase noise power spectral density to carrier ratio is about the same as the amplifier thermal noise power spectral density to signal ratio, the 2 GHz phase noise for offset frequencies greater than 1 kHz must be less than -65 dBc/Hz. This specification also fixes the low frequency noise as will be shown.

3. A frequency accuracy of $\Delta f_c/f_c$ yields a range accuracy of $\Delta r/r$. Achievable frequency stabilities of $10^{-7}$ over the mission life of GAMES limits the absolute range accuracy to about 2 mm over the mission life time.

The range rate requirement is challenging, but should be possible. Typical long term drift rates are about $10^{-6}$/year. Sami Asmar, JPL, says frequency stability

| | |
|---|---|
| $f_c = 2$ GHz | exactly |
| $\omega_c = 2\pi f_c$ | exactly |
| $f_c + \Delta f_c$ | be the actual oscillator frequency |
| $\Delta\omega_c = 2\pi\,\Delta f_c$ | |
| $r(t)$ | be the actual range |
| $v(t)$ | be the actual velocity difference between the crafts |
| $\Delta r$ | be the required absolute range resolution |
| $\Delta v$ | be the required absolute velocity resolution |
| $\alpha_T(t)$ | transmitted phase |
| $\alpha_R(t)$ | received phase |
| $\Delta\alpha$ | difference between transmitted and received phase |
| $\Delta\alpha_r$ | change in $\Delta\alpha$ due to a range change |
| $\Delta\alpha_f$ | change in $\Delta\alpha$ due to a frequency change |
| $c$ | The speed of light in vacuum. |

Table 1: Symbols used in this section.

of $10^{-13}$ may be possible over several tens of seconds. Reference [2], page 219 reports aging rates of $10^{-11}$/day.

The phase noise specification is satisfied by most oscillators, even after frequency multiplication to 2 GHz. Note that this requirement implicitly specifies the low frequency noise as is discussed later.

The absolute frequency stability is a goal, rather than a requirement. It may be possible to measure the oscillator frequency with the GPS system and correct for long term drift. Absolute ranging would then be improved if required.

See appendix for derivation of these requirements.

GAMES will have a calibration path which in principle could be used to detect frequency changes. Substituting the calibration path time delay, $\tau_c$, for the range path delay $2r/c$ in equation (24) gives the calibration phase shift as

$$\alpha_c + \Delta\alpha_c = 2\pi[f_c + \Delta f_c]\tau_c \tag{5}$$

The change in calibration path phase due to a frequency change is then given by $\Delta\alpha_c = 2\pi\,\Delta f_c \tau_c$. The ratio of calibration phase change to range phase change is

$$\frac{\Delta\alpha_c}{\Delta\alpha_f} = \frac{\tau_c}{\tau_d} \tag{6}$$

where $\tau_d$ is the inter satellite round trip range time delay. The calibration time delay is likely to be 10 ns to 100 ns. The range delay is about 1 ms. Therefore the calibration channel will then be $10^{-4}$ to $10^{-5}$ times less sensitive to frequency changes than the ranging channel and using the reference path to correct for frequency variations is not feasible.

# 3 Oscillators

## 3.1 Introduction to Quartz Crystal Oscillators

Quartz crystal oscillators are used as the frequency selective filter in oscillator circuits. Because quartz is piezo-electric, an oscillating electric field can generate acoustic waves which can in turn generate an oscillating electric field. The resonator $Q$ can be very large and is highly frequency selective. Quartz crystals can operate over the frequency range 100 kHz to 150 MHz.[11, Page 57] The crystal may be cut in one of several ways, each with advantages and disadvantages. The most common cut is AT, in which the crystal is cut once along the crystal axis. AT cut crystals are inexpensive but not as stable as SC (stress compensated) cut crystals which require two cuts in directions not parallel to any crystal axis. SC cut crystals have reduced temperature and vibration sensitivity, better short-term stability, lower aging rates, and higher immunity to radiation than AT crystals[2, Page 227].

As a quartz crystal is used, its frequency changes with time. There are three major components to the change, called drift or aging[2, Chapter 12]. After being off, there is a frequency drift as the crystal reaches thermal equilibrium. This takes a few tens of minutes to hours. Then over the next few days, the frequency changes as impurities, which condensed on the crystal while it was off, are driven off. Finally, the frequency drifts as the crystal relaxes. When the crystal is new, surface stress induced by crystal cutting relax causing frequency changes. Also the internal inter-atomic restoring forces weakened with use. This drift can be well characterized. It tends to be rapid when the crystal is new. After one or two years, the aging rate decreases to a steady, low value. In GAMES, only the last drift effect will be important since the oscillator will be run continuously. Drift rates and high frequency phase noise can be traded for each other. See the paragraph before equation (12)

Generally low frequency crystal oscillators have long term drift rates (aging

rates) lower than high frequency oscillators because the lower frequency crystals tend to be larger. With more material, the restoring forces are distributed over more atoms and the weakened bonds have a proportionally smaller effect. Large crystals can be used as high frequency resonator by operating on a vibration mode above the fundamental, known as overtones. Therefore many crystals are operated on the third or fifth overtone. It should be noted that overtone frequencies are not harmonics of the fundamental

## 3.2 Oscillator Noise

In addition to long term frequency drift, oscillators have random fluctuations in frequency, phase, and amplitude. Here amplitude noise will be ignored. Let the output of an oscillator with angular frequency $\omega_o$ be described by either

$$v(t) = v_0 \sin(\int^t \omega_o(t')dt' + \phi_o) \tag{7a}$$

$$v(t) = v_0 \sin(\omega_o t + \phi(t)) \tag{7b}$$

where $v_0$ is the amplitude. Equation (7a) describes the oscillator imperfections in terms of fluctuations in frequency, $\omega_o(t)$. Equation (7b) describes the oscillator output is terms of an average frequency, $\omega_o$, and random phase fluctuations, $\phi(t)$. Generally (7a) is used for low frequency variations, less than 0.1 Hz, while (7b) is used for high frequency variations, greater than 100 Hz. Either may be used in the transition region.

Oscillator frequency noise may be described in terms of the Allan variance. Let the oscillator frequency be measured during each of $N$ adjacent time intervals of length $\tau$. Let $f_k$ be the frequency measured during the $k$'th interval. The Allan variance is defined by

$$\sigma_f^2(\tau) = \frac{1}{2(N-1)} \sum_{k=1}^{N-1} (f_{k+1} - f_k)^2 \tag{8}$$

The Allan variance can be normalized to the carrier frequency by dividing by the square of the average frequency. The Allan variance can be converted to frequency space and plotted in terms of frequency offset from the carrier. Generally, however, it is left as a function of the measurement interval, $\tau$, which typically ranges from a few tens of milliseconds to a thousand seconds. Aging frequency changes are removed before the Allan variance is computed.

Oscillator noise may instead be described in terms of phase noise by starting with (7b). The sin(·) term is expanded to yield

$$v(t) = v_0 \{\sin(\omega_o t)\cos(\phi(t)) + \cos(\omega_o t)\sin(\phi(t))\} \tag{9}$$

Assuming that $\phi(t)$ is always small, $\cos(\phi(t))$ can be approximated as unity while $\sin(\phi(t))$ can be approximated by its argument. Thus (9) can be written as

$$v(t) \approx v_0 \sin(\omega_o t) + v_0 \cos(\omega_o t)\phi(t) \tag{10}$$

The power spectrum of $v(t)$ can be computed as

$$V(\omega) \approx \frac{v_0^2 \delta_d(\omega_o + \omega)}{4} + \frac{v_0^2 \delta_d(\omega_o - \omega)}{4} + \frac{v_o^2 S_\phi(\omega_o \pm \omega)}{2} \tag{11}$$

where $\delta_d(\cdot)$ is the Dirac delta function and $S_\phi(\omega)$ is the phase noise power spectrum. Note that this is an approximation that depends on $\phi(t) \ll 1$ and therefore can not be used at frequencies very near the carrier.

Typically the phase noise is specified as the ratio (in dB) of noise power in a bandwidth to the carrier power, $v_0^2/4$ at a frequency from the carrier, $\omega_m = \omega \pm \omega_o$. This is known as dBc.

Conversions can be made between phase noise power spectral density and frequency noise power spectral density as described in [11, Chapter 9].

The phase noise power spectrum can be divided into three regions[11, Section 5.3] as shown in Figure 1. At frequencies far from the carrier, large $\omega_m$, the power spectrum is flat due to flat, thermal noise in the oscillator amplifiers. Generally this noise to carrier ratio can be decreased by running the oscillator at higher power levels. However, higher power levels in the crystal tend to increase the crystal aging rate because of the larger vibration amplitudes. At frequencies closer to the carrier, the phase noise to carrier ratio is given by

$$\frac{S_\phi(\omega_m)}{C} \propto \frac{1}{Q^2}\left(\frac{\omega_o}{\omega_m}\right)^2 \tag{12}$$

where $\omega_m$ is the frequency offset from the carrier and $Q$ is the crystal resonator $Q$[11, Page 53]. At frequencies even closer to the carrier, the phase noise increases as $1/\omega^3$ due to flicker noise,[11, Page 53] random walk of frequency. The Transition frequency, the intercept between the $1/\omega_m^2$ and $1/\omega_m^3$ lines, depends on the flicker

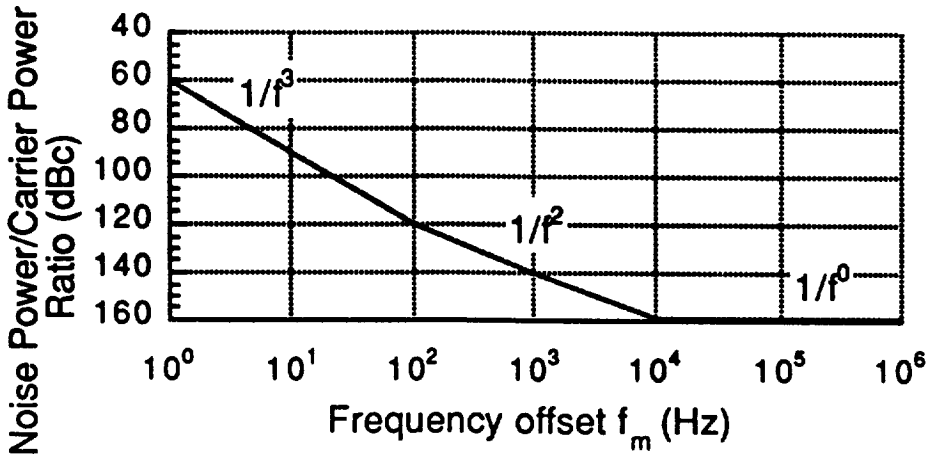


Figure 1: Typical phase noise power spectrum showing the three regions: $1/f^3$, $1/f^2$, and the flat, white noise parts.

noise of the circuit components. It should be noted that sometimes the white or flicker parts of the spectrum are so large that the $1/f^2$ part does not appear.

The power spectral density in each region can be written as

$$S_\phi(\omega_m) = a_n \left(\frac{\omega_{m_n}}{\omega_m}\right)^n \tag{13}$$

where $n = 0, 2,$ or 3 and $a_n$ is the power spectral density at frequency $\omega_m = \omega_{m_n}$. Suppose that $\omega_{m_0}$ is the angular frequency at which the flat spectrum intercepts the $1/f^2$ spectrum (or the $1/f^3$ if there is no $1/f^2$). In Figure 1, $\omega_{n_0}$ is $2\pi$ 10 kHz. Then the spectrum can be bounded by

$$S_\phi(\omega_m) \leq \begin{cases} a_0 & , \omega_m \geq \omega_{m_0} \\ a_0 \left(\frac{\omega_{m_0}}{\omega_m}\right)^3 & , \omega_m \leq \omega_{m_0} \end{cases} \tag{14}$$

This proves the surprising result that specifying the high frequency phase noise bounds the low frequency phase noise.

Recall that the entire phase noise analysis depends on the assumption of small amplitude phase noise. At some low frequency, often it is in the 1 Hz to 10 Hz range, this assumption breaks down and the system is no longer linear as is required for a Fourier description of the system. Low frequency phase noise is best described in the time domain.

Frequency multiplication by $N$ increases the phase noise power by $N^2$, the same as increasing the oscillator frequency. Therefore, assuming the crystal $Q$ is frequency independent running the oscillator at a higher frequency has the same impact on phase noise as multiplying the frequency. In general, however, the $Q$ is frequency dependent, decreasing at high frequency, and there may be an advantage in frequency multiplying.

## 3.3 Power Spectrum of Phase Differences

As described in the introduction, the distance measurement is computed from the phase difference $\Delta\alpha(t)$ which depends on $\phi(t)$ and $\phi(t - \tau_d)$. Clearly the two phases are correlated so the power spectrum of the phase difference can not be the same as the phase noise itself. It can be shown[11, Section 10.1] that the phase difference power spectrum, $S_{\Delta\alpha}(\omega_m)$, is related to the phase noise power spectrum, $S_\phi(\omega_m)$, by

$$S_{\Delta\alpha}(\omega_m) = 4S_\phi(\omega_m)\sin^2\left(\frac{\omega_m\tau_d}{2}\right) \tag{15}$$

It is convenient to bound the power spectral density by using the relations that for all $x$, $\sin^2 x \leq x^2$ and $\sin^2 x \leq 1$ which yields a bound given by

$$S_{\Delta\alpha}(\omega_m) \leq \begin{cases} S_\phi(\omega_m)(\omega_m\tau_d)^2 & , |\omega_m| \leq 2\tau_d^{-1} \\ 4S_\phi(\omega) & , |\omega_m| \geq 2\tau_d^{-1} \end{cases} \tag{16}$$

Substituting (13) into (16) yields

$$S_{\Delta\alpha}(\omega_m) \leq \begin{cases} a\omega_{mn}^n\tau_d^2\omega_m^{2-n} & , |\omega_m| \leq 2\tau_d^{-1} \\ 4S_\phi(\omega) & , |\omega_m| \geq 2\tau_d^{-1} \end{cases} \tag{17}$$

where, as before, $n = 0, 2$, or $3$, is the exponent appropriate for the frequency. For frequencies less than the inverse delay time, the phase difference power spectrum is reduced by differencing. Unfortunately, the low frequency, $n = 3$, spectrum still grows as $1/\omega_m$. As will be shown, this effect is not important for velocity measurements although it is important for range measurement.

The phase difference variance, $\sigma_{\Delta\alpha}^2$ is bounded by the integral of (17) over all frequencies.

$$\sigma_{\Delta\alpha}^2 \leq 2\int_0^\infty S_{\Delta\alpha}(\omega_m)d\omega_m \tag{18}$$

Unfortunately, the integral in (18) is infinite. As usual, a high frequency cutoff is imposed by the system electronics. But the $1/\omega_m$ factor still generates a divergence

at low frequencies without an obvious cutoff frequency except for the breakdown of the small phase error assumption. Fortunately the velocity variance is bounded and decreases with increasing observation time as shown next.

At low offset frequencies, the difference phase variance is given by

$$\sigma_{\Delta\alpha}^2 \approx a\omega_0^2\tau_d^2 \int_{B_1}^{B_2} \frac{d\omega_m}{\omega_m} \tag{19}$$

where $B_{1(2)}$ are the low (high) frequency limits of integration and observation. The range variance is related to the difference phase variance by $\sigma_r^2 = \sigma_{\Delta\alpha}^2(\lambda/4\pi)^2$ where $\lambda$ is the modulation wavelength. As the observation period increases, $B_1 \rightarrow 0$, the range variance increases without bound. Defining $T_{1(2)} = 1/B_{1(2)}$, the range variance may be expressed as a function of the observation time as $a\omega_0^2\tau_d^2 \ln(T_2/T_1)(\lambda/4\pi)^2$. The velocity error is then given by

$$\sigma_v^2 = 2\frac{\sigma_r^2}{T_2^2} = \frac{2a\omega_o^2\tau_d^2 \ln\left(\frac{T_2}{T_1}\right)}{T_2^2}\left(\frac{\lambda}{4\pi}\right)^2 \tag{20}$$

For increasing observation time, $T_2 \rightarrow \infty$, the velocity error goes to zero.

As a particular example, assume that an oscillator just satisfies the high frequency phase noise requirement and the phase noise $1/f^3$ dependence starts at 1 kHz. Then $a \leq -65$ dBc/Hz and $\omega_0 = 2\pi \times 1$ kHz. Let $\lambda = 150$ mm and $\tau_d = 1$ ms which is appropriate for the fine ranging system at maximum satellite separation. Then the velocity error is given by

$$\sigma_v = \frac{60\mu\text{m}}{T_2}\sqrt{\ln(T_2/T_1)} \tag{21}$$

The second factor is of order unity. For example, $\sqrt{\ln(10^{10})} = 4.8$. Let $T_1 = 1$ ms. which is a very conservative estimate of the upper frequency response for the measurement. Over 1 second periods, $T_2 = 1$ s, the velocity error is $160\mu$m/s. For $T_2 = 10$ s, the velocity error is $18\mu$/s. Over 100 s, the velocity error is $2\mu$m/s. So the $1/\omega^3$ phase noise is not likely to be a major problem. However it is also likely that the phase model is not very accurate over such long time periods.

# 4 Conclusions

Table 2 shows some specifications of commercially available oscillators. Figure 2 plots the phase noise spectrums. The $\omega_m^{-3}$ dependence is clearly visible in the TRAK

| Maker | Frequency | Frequency Stability | Drift Rate | Phase noise (dBc) at 10 Hz | 100 Hz | 1 kHz |
|---|---|---|---|---|---|---|
| TRAK | 2 GHz | $5 \times 10^{-6}$ | $5 \times 10^{-6}$/year | -55 | -85 | -105 |
| Efratom/Ball | 10 MHz | $5 \times 10^{-12}$/s | | -74 | -94 | -104 |
| Wenzel | 10 MHz | | $1 \times 10^{-9}$/day | -89 | -109 | -119 |

Table 2: Specifications of some commercially available crystal oscillators. The phase noise specifications are after perfect multiplication to 2 GHz.

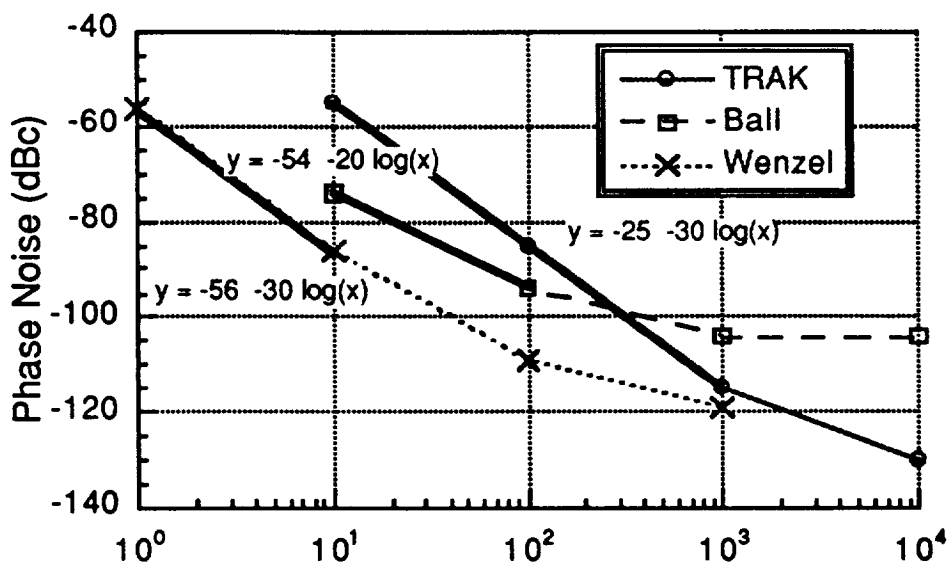


Figure 2: Phase noise power spectral density for three commercial oscillators: One from TRAK, Efratom/Ball, and Wenzel. Phase noise adjusted to 2 GHz frequency when required. Also shown are the fits to the lowest frequency values.

and Wenzel oscillators. All three oscillators easily satisfy the high frequency phase noise requirement. Also, extending the low frequency fits to 1 kHz gives $a < -110$dBc for all three which yields velocity errors more than 100 times smaller than in the example of the previous section.

Assuming that the frequency stability and drift rates can be extended linearly to different time spans, either the Efrtom/Ball or the Wenzel oscillator will satisfy or nearly satisfy the GAMES oscillator performance requirements. However more information is needed on the stability to be sure.

# Derivation of stability equations

These appendixes derives the equations used in section 2 to compute the master oscillator frequency and phase stability requirements. First the frequency stability required for the velocity measurement is computed. The frequency variations may be either long term drift or random fluctuations. Then the phase stability requirement is derived. Finally, the effect of frequency variations on the absolute range measurement is derived. This will bound the absolute inter-satellite range measurement over the life of the GAMES mission.

# A Derivation of required frequency stability

First the effect of frequency drift on the velocity measurement is determined. Assume that the frequency is exactly $f_c$ and the relative velocity is zero. Then

$$\Delta\alpha = \frac{2\pi f_c 2r}{c} \tag{22}$$

If the range changes by $\Delta r$ then the new difference phase will be

$$\Delta\alpha + \Delta\alpha_r = \frac{2\pi f_c 2[r + \Delta_r]}{c} \tag{23}$$

where $\Delta\alpha_r$ is the change of phase due to a range change and is given by $2\pi f_c 2\Delta r/c$. If the frequency were to change instead from $f_c$ to $f_c + \Delta f_c$ the new difference phase would be

$$\Delta\alpha + \Delta\alpha_f = \frac{2\pi[f_c + \Delta f_c]2r}{c} \tag{24}$$

where $\Delta\alpha_f$ is the change due to the frequency change and is given by $2\pi\Delta f_c 2r/c$. For $\Delta r$ to be the resolution limit, must have $\Delta\alpha_f \leq \Delta\alpha_r$ or

$$\frac{\Delta f_c}{f_c} \leq \frac{\Delta r}{r} \tag{25}$$

as claimed in item 1.

# B Derivation of maximum frequency drift

To measure the range rate to a specified accuracy requires that the error in the range measurement grow no more rapidly than the desired range rate. Assume that it is desired to measure the range rate over a time period $\Delta t$ to an accuracy of $\Delta v$. Two range measurements, each with accuracy $\Delta r$, are required. If $\Delta r$ is the range measurement standard deviation, then the velocity error is $\Delta v = \sqrt{2}\Delta r/\Delta t$. If $\Delta r$ is the peak error, then the velocity error is $\Delta v = 2\Delta r/\Delta t$. Because the latter provides a tighter bound, it will be used. Then the range error permitted for each measurement will increase as $\Delta r = \Delta t \Delta v/2$. Assume that the oscillator frequency is exactly $f_c$. At time $t$, the difference phase is measured as

$$\Delta\alpha = \frac{2\pi f_c 2r}{c} \tag{26}$$

Assume that during the time interval $t$ to $t + \Delta t$ the range increases to $r + \Delta r$. The new difference phase measured at time $t + \Delta t$ is

$$\Delta\alpha + \Delta\alpha_r = \frac{2\pi f_c 2[r + \Delta v \Delta t]}{c} \tag{27}$$

for a change of $\Delta\alpha_r = 2\pi f_c \Delta v \Delta t/c$ and a time rate of change of the difference phase of

$$\frac{\Delta\alpha_r}{\Delta t} = \frac{2\pi f_c}{c} 2\Delta v \tag{28}$$

If the range did not change, but the oscillator frequency changes from $f_c$ to $f_c + \Delta f_c$, then there will be a difference phase change to

$$\Delta\alpha + \Delta\alpha_f = \frac{2\pi[f_c + \Delta f_c]2r}{c} \tag{29}$$

Therefore the time rate of change of the difference phase is given by

$$\frac{\Delta\alpha_f}{\Delta t} = \frac{2\pi\,\Delta f_c}{c\Delta t}2r \tag{30}$$

For the desired phase shift $\Delta\alpha_r$ can be observed, it must be true that $\Delta\alpha_f/\Delta t \leq \Delta\alpha_r/\Delta t$ or

$$\frac{\Delta f_c}{f_c\Delta t} \leq \frac{\Delta v}{r} \tag{31}$$

as claimed in 2. It makes no difference if the frequency drifts gradually during the time interval, wonders randomly during the interval, or experiences a step frequency change.

# C Derivation of required phase stability

So far, attention has focused on frequency changes. Now the attention turns to phase noise which has two effects. In a standard Doppler radar system, phase noise of the master oscillator decreases the dynamic range of the doppler system. When a strong reflector and a weak reflector are both in the radar field of view and have similar doppler shifts, the weak reflector will be hidden in the reflected strong signal. Because GAMES has only one target in the field of view, this is not a problem.

Phase noise will also introduce a random component to the phase measurement. For frequencies offset from the carrier by more than ≈1 kHz, the received and reference phase are uncorrelated. The phase noise must be an insignificant component to the total noise budget. I will specify that the phase noise power spectral density is about the same or smaller than the thermal noise from the PMT pre-amplifier. However, it should be remembered that the phase noise is proportional to the signal power and will increase with signal power or PMT gain.

The phase noise power density (dBc/Hz) should be about the same as the amplifier thermal noise to signal ratio (dBsignal/Hz). Xiaoli Sun reports the signal power from the PMT as $5.5 \times 10^{-16} A^2$. The noise current of a 50Ω resistor is given by $i^2 = NFk_BT/R_L$ where $NF$ is the noise factor, here assumed 2 times. The noise current is $1.6 \times 10^{-22} A^2$/Hz. Therefore the thermal noise to signal ratio is -65 dB/Hz which is about what the phase noise at 2 GHz must be, -65 dBc/Hz. This specification is easy to meet. Most crystal oscillators have phase noise densities smaller than -80 dBc, even after frequency multiplication to 2 GHz.

# References


[1] Baghdady, E. G., Lincoln, R. N., and Nelin, B. D., Short-Term Frequency Stability:Characterization, Theory, and Measurement, *Proc. IEEE*, **53**, page 704-722 (1965) Reprinted in [6]

[2] Bottom, V. E., *Introduction to Quartz Crystal Unit Design*, Van Nostrand Reinhold Company, (1982)

[3] Driscoll, M. M., Low Frequency Noise Quartz Crystal Oscillator, *Trans. on Instr. and Meas.*, **IM-24**, Page 21–26, (1075)

[4] Frerking, M. E., *Crystal Oscillator Design and Temperature Compensation*, Van Nostrand Reinhold Company, (1978)

[5] Goldman, S. J., *Phase Noise Analysis in Radar Systems Using Personal Computers*, John Wiley & Sons, (1989)

[6] Kroupa, V. F., *Frequency Stability: Fundamentals and Measurement*, IEEE, (1983)

[7] Kroupa, V. F., *Frequency Synthesis: Theory, Design and Applications*, John Wiley & Sons, (1973)

[8] *Precision Measurement and Calibration:Frequency and Time*, National Bureau of Standards #300 V5, (1972)

[9] *Time and Frequency Users' Manual*, National Bureau of Standards #559, (1979)

[10] Raven, R. S., Requirements on Master Oscillators for Coherent Radar, *Proc. of the IEEE*, **54**, Page 237–243 (1066)

[11] Robins, W. P., *Phase Noise in Signal Sources: Theory and Applications*, IEEE, (1982)

[12] Stirling, R. C., *Microwave Frequency Synthesizers*, Prentice–Hall, Inc., (1987)

# Sample Rate and Number of Bits Required for the GLAS Waveform Digitizer

Xiaoli Sun/JHU, December 19, 1994

A minimum sample rate and the vertical resolution is derived for the waveform digitizer in the GLAS receiver. It shows that a 0.8-1 Gs/s 6 bit A to D converter is sufficient to achieve the require ranging performance.

## 1. The Sample Rate of the GLAS Waveform Digitizer

The sample rate of the GLAS waveform digitizer should be chosen such that the ranging error caused by the finite sample rate is negligible as compared with other sources of errors. The required ranging accuracy for GLAS is 5 cm for a roughly 30 ns wide received pulse (3° slope, 70m diameter laser foot print, and 5 ns wide laser pulses). The current design of the GLAS receiver sets the sample rate to 3 Gs/s, which corresponds to a range bin of 5 cm. This choice of the sample rate is supported by the analysis given by Gardner[1], which says the sample interval should be about 1/10 the rms pulse width. Since the laser pulse width for GLAS is 5 ns FWHM, the rms pulse width is $2.5\text{ns}/(2\ln(2))^{1/2} = 2.13\text{ns}$. Assuming the impulse response of the photodetector has the same pulse width, the minimum rms pulse width of the signal into the waveform digitizer is $(2.13^2 \times 2.13^2)^{1/2} = 3.01$ ns. Therefore, the required sample rate would be about 3.3 GHz according Gardner's analysis.

On the other hand, since the input signal is band limited, the sample rate needs only to be twice the reciprocal of the bandwidth according to Nyquist Theorem. The 3dB bandwidth of the GLAS photodetector is about 150 MHz, the stop band (-30dB) frequency is about 400 MHz assuming a >20dB/octave roll off response. Therefore, the sample rate needs only to be 0.8 Gs/s. Lower sample rate would mean less electronics, lower power consumption, and possibly less signal processing time. In theory, one could completely reconstruct the waveform by taking the Discrete Fourier Transform

(DFT) of the samples and then a regular inverse Fourier transform of the center segment of the DFT.

If the general pulse shape is known, even fewer samples are needed to recover the pulse shape. Ideally, the number of samples need only to be equal or greater than the number of unknown parameters of the received pulse shape. For example, three samples would be necessary if the pulse shape were Gaussian with unknown time delay, width, and amplitude and no noise. More samples are required in practice in order to average out the noises. The parameter values of the received pulse can be obtained through a standard data fitting technique, such as maximum likelihood or minimum mean square error data fitting. In general, the timing accuracy can always be much smaller than the sampling interval unless the pulses are perfect rectangle with zero rise and fall times. As an example, the LeCroy LW410/420 arbitrary waveform generator can form a time shift in its output waveform by as little as 100 ps, a small fraction of the 2.5 ns sampling interval, with 8 bit vertical resolution[2].

For GLAS, no assumption can be made about the exact pulse shape since they represent the features of the ground target to be studied. The sample rate must be determined based on the transmitted laser pulse shape and the receiver impulse response. Intuitively, the sample rate has to cover the rate of change of the received signal. Based on this principle, the sampling interval has to be a fraction of the pulse rise and fall times. Since the GLAS detector has a 3 dB bandwidth of 150 MHz, the rise time of the output signal is at most 0.35 times the reciprocal of the bandwidth, or 2.3ns. We can safely set the sample rate to 850 Ms/s which gives two samples per rise time. This sample rate is also close to that given by the Nyquist Theorem. One could reconstruct the received pulse to a great accuracy by connecting the samples using standard linear or cubic spline interpolation. The centroid of the received pulse which gives the range of the ground target may be calculated approximately by summing all the samples weighted by their arrival times. One may

further improve the ranging accuracy by using the Simpson's rule in the summation, as in the theory of numerical integration.

In conclusion, the 3Gs/s sample rate for the GLAS waveform digitizer is shown to be excessive and the suggested is 0.8-1 Gs/s. The analysis given by Gardner about the quantization error appears to be inaccurate. An exact analysis of the ranging error due to the sampling rate seems difficult. A numerical solution may be obtained through a computer simulation using the GLAS simulator. The ultimate solution has to come from the test results of the GLAS breadboard receiver.

## 2. The Number of Bits of the GLAS Waveform Digitizer

The finite step size of the A/D converter causes a quantization error in each sample of the output. The quantization errors may be modeled as identically and independently distributed random variable and they all follow a uniform distribution of the digitizer step size[3].

The output of the waveform digitizer may be written as

$$y(n) = x(n\Delta t) + e_i = x(n) + e_i$$

with x(t) the input analog signal, $\Delta t$ the sampling interval, and $e_i$ the quantization error. The measured target range is proportional to centroid of the received pulse, which can be written as

$$T_c = \frac{\sum_i i\Delta t\, y(i)}{\sum_i y(i)} = \Delta t \cdot \frac{\sum_i i \cdot x(i) + \sum_i i \cdot e_i}{\sum_i x(i) + \sum_i e_i}$$

$$= \Delta t \cdot \frac{\sum_i i \cdot x(i)}{\sum_i x(i)} \cdot \frac{\left(1 + \sum_i i \cdot e_i \Big/ \sum_i i \cdot x(i)\right)}{\left(1 + \sum_i e_i \Big/ \sum_i x(i)\right)}$$

Assuming the quantization errors are small compared to the average pulse amplitude, i.e., $\sum_i e_i \Big/ \sum_i x(i) << 1$, the pulse centroid may be approximate as

$$T_c \approx \Delta t \cdot \frac{\sum_i i \cdot x(i)}{\sum_i x(i)} \cdot \left( 1 + \frac{\sum_i i \cdot e_i}{\sum_i i \cdot x(i)} \right)$$

The quantization error normalized with respect to the rms pulse width, $\sigma_p$, is given by

$$\varepsilon = \frac{\sqrt{\mathrm{var}\{T_c\}}}{\sigma_p} = \frac{1}{\sigma_p} \sqrt{\mathrm{var}\left\{ \Delta t \cdot \frac{\sum_i i \cdot e_i}{\sum_i x(i)} \right\}} = \frac{\Delta t}{\sigma_p} \cdot \frac{\frac{\Delta x}{\sqrt{12}} \sqrt{\sum_i i^2}}{\sum_i x(i)}$$

where $\Delta x = x_{max}/2^N$ is the step size, $x_{max}$ is the full scale voltage, and N is the number of bits.

We further assume that the received pulse shape is Gaussian, i.e., $x(n) = x_0 \exp\{-(n\Delta t)^2/2\sigma_p^2\}$ with $x_0$ the peak pulse amplitude. The summation in the centroid calculation is assumed to extends to $\pm 2\sigma_p$. The scaling factor of the waveform digitizer is chosen such that $x_{max} = \alpha x_0$ with $\alpha \geq 1$ the dynamic range. Under these conditions, the quantization error becomes

$$\varepsilon \approx \frac{\Delta t}{\sigma_p} \cdot \frac{\alpha}{2^N \sqrt{12}} \cdot \frac{\sqrt{\sum_{i=-2\sigma_p/\Delta t}^{2\sigma_p/\Delta t} i^2}}{\sum_{i=-2\sigma_p/\Delta t}^{2\sigma_p/\Delta t} e^{-\frac{(i\Delta t)^2}{2\sigma_p^2}}} \approx \frac{\Delta t^2}{\sigma_p^2} \cdot \frac{\alpha}{2^N \sqrt{12}} \cdot \frac{1}{\sqrt{2\pi}} \cdot \sqrt{\frac{2\sigma_p}{3\Delta t}\left(\frac{2\sigma_p}{\Delta t} + 1\right)\left(\frac{4\sigma_p}{\Delta t} + 1\right)}$$

$$\approx \frac{1}{3}\sqrt{\frac{2}{\pi}} \cdot \frac{\alpha}{2^N} \cdot \sqrt{\frac{\Delta t}{\sigma_p}}$$

To calculate the required number of bits for GLAS, we assume $\sigma_p = 13$ns (30ns FWHM pulse width) and $\Delta t = 1$ ns (1Gs/s). The quantization error for a 8 bit A/D converter with 3dB dynamic range ($\alpha = 2$) is $\varepsilon \approx 5.76 \times 10^{-4}$.

The relative ranging error required by GLAS is

$$\varepsilon_{max} = \frac{2\frac{5cm}{c}}{13ns} = 2.56\%$$

The quantization error has to be much smaller than $\varepsilon_{max}$. If we choose $\varepsilon=\varepsilon_{max}/10$, the number of bits required is 6 bits. An 8 bit A/D converter will give a dynamic range of $\alpha$ =8 (18dB).

The desired dynamic range for GLAS receiver is 26dB, which accounts for a factor of 10 variation in the ground reflectivity and a factor of two APD gain fluctuation. Therefore, an automatic gain control (AGC) amplifier is still required in front of the waveform digitizer.

REFERENCES

1. C. S. Gardner, 'Ranging performance of satellite laser altimeters,' *IEEE Trans. Geoscience and Remote Sensing*, Vol. 30, No. 5, pp. 1061-1072, Sept. 1992.

2. 'Precise waveform time shifts, moving waveform peaks and edges with increments -100ps,' Application Brief, No. L.A.B. 902, LeCroy Corp.

3. A. V. Oppenheim and R. W. Schafer, *Discrete-Time Signal Processing*, Prentice-Hall, Englecliff, NJ, 1989, p. 119.